LIMITS ON THE WIMP-NUCLEON CROSS-SECTION FROM THE CRYOGENIC DARK MATTER SEARCH

R.J. GAITSKELL (FOR THE CDMS COLLABORATION*)
Department of Physics and Astronomy, University College London, Gower St, London WC1E 6BT, UK. E-mail: rick@gaitskell.com

The Cryogenic Dark Matter Search (CDMS) employs Ge and Si detectors to search for WIMPs via their elastic-scattering interactions with nuclei while discriminating against interactions of background particles. CDMS I data, from the Stanford Underground Facility shallow site, give limits on the spin-independent WIMP-nucleon elastic-scattering cross-section that exclude unexplored parameter space above 10 GeV c^{-2} WIMP mass and, at $> 75\%$ CL, the entire 3σ allowed region for the WIMP signal reported by the DAMA experiment. The move to a deep site at Soudan, Minnesota, should improve the experiment's sensitivity by $\sim 100\times$. "First Dark" for CDMS II will be in 2001.

We will spare you the usual preamble concerning the evidence for nonluminous, nonbaryonic, "cold" dark matter, since this will be more than adequately covered in these proceedings. The CDMS experiments (I and II) are looking for one possible, and well motivated, candidate, the WIMP (Weakly Interacting Massive Particle). Minimal supersymmetry provides a natural WIMP candidate in the form of the lightest superpartner, with a typical mass $M \sim 100$ GeV c^{-2}, and an expected event rate in terrestrial detectors that is model-dependent but is generically 1 kg^{-1} d^{-1} or lower. [1]

The purpose of the Cryogenic Dark Matter Search (CDMS) is to measure or constrain the spin-independent WIMP-nucleon elastic-scattering cross-section by extended exposure of semiconductor detectors that discriminate WIMP-induced nuclear recoils from electron recoils caused by interactions of

*D.S. AKERIB, A. BOLODYZNYA, D. DRISCOLL, T.A. PERERA, R.W. SCHNEE FROM CWRU; M.B. CRISLER, R. DIXON, S. EICHBLATT, D. HOLMGREN FROM FERMILAB; J. EMES, E.E. HALLER, R.R. ROSS, A. SMITH, J.D. TAYLOR FROM LBNL; K.D. IRWIN, J.M. MARTINIS, S.W. NAM FROM NIST; T. SHUTT FROM PRINCETON U.; B.A. YOUNG FROM SANTA CLARA U.; F.P. LIPSCHULTZ, B. NEUHAUSER, P. SHESTOPLE FROM SFSU; R. ABUSAIDI, P.L. BRINK, B. CABRERA, J.P. CASTLE, C. CHANG, R.M. CLARKE, P. COLLING, A.K. DAVIES, B. DOUGHERTY, M. PENN, T. SAAB FROM STANFORD U.; P.D. BARNES, JR., A. CUMMINGS, A. DA SILVA, R.J. GAITSKELL, S.R. GOLWALA, J. HELLMIG, J. JOCHUM, V. MANDIC, P. MEUNIER, M.C. PERILLO-ISAAC, B. PRITYCHENKO, B. SADOULET, D.N. SEITZ, G.W. SMITH, A.L. SPADAFORA, W. STOCKWELL, S. WHITE FROM UC BERKELEY; D.A. BAUER, R. BUNKER, D.O. CALDWELL, D. HALE, C. MALONEY, H. NELSON, J. SANDER, A.H. SONNENSCHEIN, S. YELLIN FROM UC SANTA BARBARA; M.E. HUBER FROM U. OF COLORADO.

background particles The ionization yield Y (the ratio of ionization production to recoil energy of a particle interaction) differs greatly for nuclear and electron recoils. The two types of CDMS detectors each measure phonon and electron-hole pair production to determine recoil energy and ionization yield for each event. With Berkeley Large Ionization- and Phonon-mediated (BLIP) detectors, phonon production is determined from the detector's calorimetric temperature change. [3,4,5] With Z-sensitive Ionization- and Phonon-mediated (ZIP) detectors, athermal phonons are collected to determine phonon production and xy-position. [2,6,7]

Above 10 keV, CDMS detectors reject bulk electron recoils with $> 99\%$ efficiency and surface events with $> 95\%$ efficiency. [9,5] CDMS detectors that sense athermal phonons provide further surface-event rejection based on the differing phonon pulse shapes of bulk and surface events. This phonon-based surface-event rejection alone is $> 99.7\%$ efficient above 20 keV. [7,8]

Key to the success of the CDMS I experiment at its current shallow site (20 mwe) is a $> 99.9\%$ efficient plastic-scintillator veto that detects muons, allowing rejection of muon-coincident events. The event rate below 100 keV in Ge due to photons is roughly 60 keV^{-1} kg^{-1} d^{-1} overall and 2 keV^{-1} kg^{-1} d^{-1} anticoincident with veto.

Neutrons with energies capable of producing keV nuclear recoils are produced by muons interacting inside and outside the muon veto ("internal" and "external" neutrons, respectively). The dominant, low-energy (< 50 MeV) component of these neutrons is moderated by a 25-cm thickness of polyethylene. [10] However, high-energy external neutrons may be unvetoed, and can punch through the moderator. In the final statistical analyses of the data we use only flux-normalization independent predictions of Monte Carlo simulations, such as relative rates of single scatters and multiple scatters, relative rates in Si and Ge detectors, and the shapes of nuclear-recoil spectra, which are also insensitive to reasonable changes in the neutron spectrum.

Two data sets are used in this analysis: one consisting of 33 live days taken with a 100 g Si ZIP detector in 1998, and another taken later with Ge BLIP detectors. [11] The Si run yields a 1.6 kg d exposure after cuts. [6,7] The total low-energy electron surface-event rate is 60 kg^{-1} d^{-1} between 20 and 100 keV. Four nuclear recoils are observed in the Si data set. An electron calibration sets the 90% CL upper limit on the expected number of misidentified surface events at 0.26 events. These nuclear recoils also cannot be due to WIMPs. Whether their interactions with target nuclei are dominated by spin-independent or spin-dependent couplings, WIMPs yielding the observed Si nuclear-recoil rate would cause an unacceptably high number of nuclear recoils in the Ge data set discussed below. Therefore, the Si data set measures

the unvetoed neutron background.

Between November, 1998, and September, 1999, 96 live days of data were obtained using 3 of 4 165 g Ge BLIP detectors. The top detector of the 4-detector stack is discarded because it displays a high rate of veto-anticoincident low-energy electron surface events, 230 kg^{-1} d^{-1} as compared to 50 kg^{-1} d^{-1} for the other detectors (10 to 100 keV). This detector appears to have been contaminated by a small amount of material from a beta calibration source. Data-quality, nuclear-recoil acceptance, and veto-anticoincidence cuts reduce the exposure (mass $\times$ time) by 45%. To take advantage of close packing, analysis is restricted to events fully contained in the inner electrodes, reducing the exposure further by a factor of 2.47 to yield a final Ge exposure of 10.6 kg d. [5]

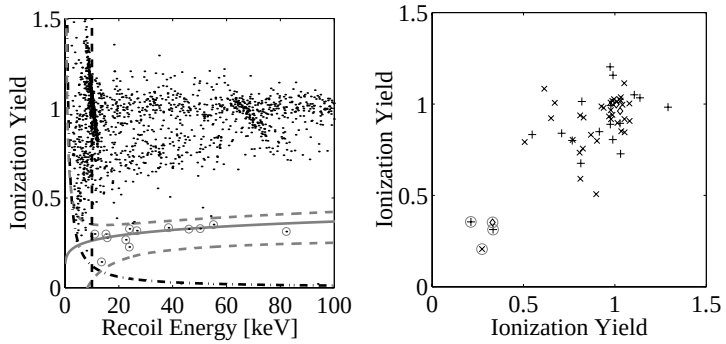

Figure 1. (**a**) Ionization yield (Y) vs. recoil energy for veto-anticoincident single scatters contained in the inner electrodes of the 3 uncontaminated Ge detectors. Thirteen events (*circled*) lie within the nominal 90% nuclear-recoil acceptance region (*dashed curves*), above both the 10 keV analysis threshold (*dashed line*) and the threshold for separation of ionization signal from amplifier noise (*dot-dashed curve*). The expected position of nuclear recoils (*solid curve*) is also shown. The presence of 3 events just above the acceptance region is compatible with 90% acceptance. (**b**) Scatter plot of ionization yields for multiple scatters in the top/middle (*crosses*), middle/bottom ($\times's$), or top/bottom (*diamonds*) uncontaminated Ge detectors with at least 1 inner-electrode scatter and both scatters between 10 and 100 keV. Four events (*circled*) are tagged as nuclear recoils in both detectors. Bulk recoils and surface events lie at $Y \approx 1$ and $Y \sim 0.75$, respectively

Figure 1 shows a plot of ionization yield vs. recoil energy for the Ge single scatters (events triggering a single detector), as well as a scatter plot of ionization yields for the Ge multiple scatters. Bulk electron recoils lie at ionization yield $Y \approx 1$. Low-energy electron events form a distinct band at $Y \sim 0.75$, leaking into the nuclear-recoil acceptance region below 10 keV. Imposing an

analysis threshold of 10 keV, well above trigger thresholds, simplifies analysis by rendering low-energy electron misidentification negligible.

Thirteen unvetoed nuclear recoils are observed between 10 and 100 keV. The Ge nuclear-recoil efficiency is above 80% throughout this energy range, and was determined *in situ* using calibration-source neutrons.

The observation of 4 Ge multiple-scatter nuclear recoils (Fig. 1b) indicates that many if not all of the unvetoed nuclear recoils are caused by neutrons rather than WIMPs, since the WIMP multiple-scatter rate is negligible. It is also highly unlikely that these events are misidentified low-energy electron events (0.03 upper bound, 90% CL). Figure 1 demonstrates excellent separation of low-energy electron events from nuclear recoils.

There is reasonable agreement between predictions for neutrons from the Monte Carlo simulation and the relative observed numbers of 4 Ge multiple scatters, 4 Si single scatters, and 13 Ge single scatters. Normalizing the simulation by the 17 total Ge nuclear-recoil events yields 3.4 expected Si single scatters and 1.0 expected Ge multiple scatters (note that these numbers have changed slightly from those in [11]).

The 90% CL excluded region for the WIMP mass M and the spin-independent WIMP-nucleon elastic-scattering cross-section σ is found using an extension of the approach of Feldman and Cousins. [13,11] The above arguments require accounting for the component of the observed Ge single scatters that is due to the unvetoed neutron flux n. This flux is constrained by the 4 multiple scatters in Ge and the 4 nuclear recoils in Si. To determine the 90% CL excluded region in the plane of M and σ alone, the parameter n is projected out. Figure 2 displays the lower envelope of points excluded for all values of n. This line corresponds to an expectation of ~ 8 WIMPs in the Ge single-scatter data set. Because all the nuclear recoils may be neutron scatters, $\sigma = 0$ is not excluded.

This limit excludes new parameter space for WIMPs with $M > 10$ GeV c^{-2}, some of which is allowed by supersymmetry. These data exclude, at $> 75\%$ CL, the entire 3σ region allowed by the DAMA/NaI-1 to 4 annual modulation signal. [12] This region, given by the $v_0 = 220$ km s^{-1} curve in Fig. 4a of [12], is used because it is determined directly from the annual modulation signal. Furthermore, a likelihood ratio test indicates the CDMS data and DAMA's model-independent signal (as shown in Fig. 2 of [12]) are incompatible at 99.98% CL in the asymptotic limit. Although without theoretical support, non-A^2 scaling or a dark matter halo significantly different from the one assumed in [14] may allow the two results to be compatible.

Figure 2 also shows explicitly the annual modulation signal amplitude ex-

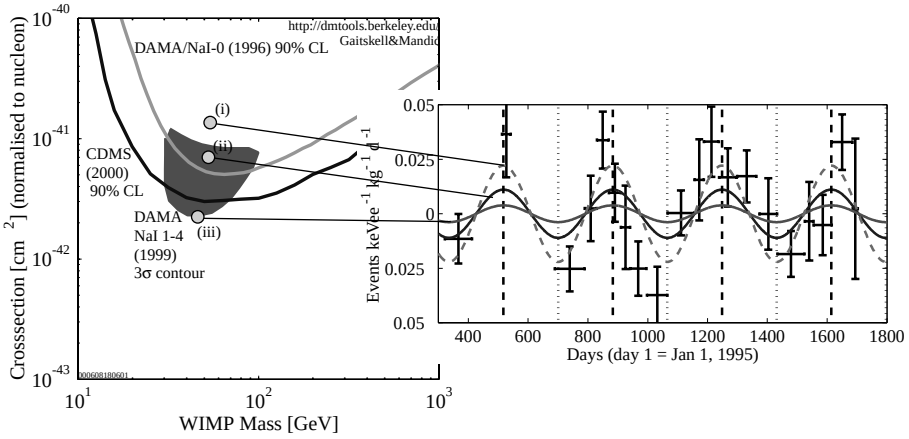

Figure 2. The left-hand side of the figure shows the spin-independent WIMP-nucleon σ vs. M plot. It includes the latest CDMS limit [11], and the DAMA 3σ allowed region. [12] On the right-hand side is a plot of the DAMA annual modulation experimental signal with error bars (taken over 4 years, for the 2-6 keVee energy bin) extracted from Figure 2 of [12]. Superimposed on the plot are the calculated modulation signals for three different WIMP scenarios identified on the σ vs. M plot. See the text for details of the cases (i),(ii) and (iii). All curves are normalized following [14], using the Helm spin-independent form-factor, A^2 scaling, WIMP characteristic velocity $v_0 = 220$ km s^{-1}, mean Earth velocity $v_{\rm E} = 232$ km s^{-1}, and WIMP density $\varrho = 0.3$ GeV c^{-2} cm^{-3}. Further sensitivity plots for many experiments are available from our automated data plotter on the web. [15]

pected in the DAMA experiment for various WIMP scenarios. For comparison we will also give the corresponding WIMP nuclear recoil (NR) event rate expected for the 10.6 kg-day CDMS Ge exposure. Three cases of WIMPs given by the (σ,M) parameters are considered: (i) (1.4 10^{-41} cm^2, 50 GeV) which represents a best fit to the DAMA NaI/1-4 annual modulation signal alone. (This was determined only from a fit to the points in Figure 2 of [12], since the underlying data is not publicly available. However, the behaviour of this fit appears to be in good agreement with the χ^2 details given in that paper.) This WIMP scenario is not within the DAMA 3σ contour because it leads to negative backgrounds predicted in the lowest energy (2-3 keVee) bins of two (out of the nine) detectors in the NaI array. By comparison, for the CDMS exposure, 40 WIMP NR events would be expected. This statistic further illustrates why the two results are incompatible at 99.98% CL in the asymptotic limit as discussed in the paragraph above. Case (ii) (7.2 10^{-42} cm^2, 52 GeV)

is the best fit in the likelihood analysis for the DAMA NaI/1-4 where their modulation and non-negative background constraints are combined. [12] The modulation amplitude is half that for (i). Case (ii) would correspond to seeing 20 WIMP events in the CDMS Ge run. The CDMS limit curve is about a factor 2.5 in σ below this scenario at this WIMP mass which corresponds to ~ 8 WIMP NR events. Finally, case (iii) ($2.5\ 10^{-42}$ cm^2, 40 GeV) corresponds to the lowest cross-section on the DAMA 3σ contour. This would correspond to ~ 6 WIMP NR events in CDMS. This scenario is consistent with the CDMS experimental result discussed in this paper. However, the very small annual modulation amplitude for this case can be seen in the right-hand plot of Figure 2, and should be compared to the amplitude of the signal actually observed in the DAMA experiment.

References

1. J. Ellis, A. Ferstl, K.A. Olive: hep-ph/0007113. J. Ellis, T. Falk, K.A. Olive, M. Schmitt: Phys. Lett. B **413**, 355 (1997). V. Mandic, A. T. Pierce, P. Gondolo, H. Murayama, hep-ph/0008022. J. Edsjo, P. Gondolo: Phys. Rev. D **56**, 1879 (1997). A. Bottino, F. Donato, N. Fornengo, S. Scopel: Phys. Rev. D **62**, 1879 (2000). R. Arnowitt, B. Dutta, Y. Santoso: hep-ph/0008336. A. Corsetti and P. Nath, hep-ph/000316. G. Jungman, M. Kamionkowski, and K. Griest, *Phys. Rep.* **267**, 195 (1996).
2. P. Brink, in these proceedings.
3. T. Shutt et al.: Phys. Rev. Lett. **69**, 3531 and 3425 (1992).
4. R. Gaitskell et al.: In *Proceedings of the Seventh International Workshop on Low Temperature Detectors*, ed. by S. Cooper (Max Planck Institute of Physics, Munich 1997).
5. S.R. Golwala: Ph. D. thesis, University of California, Berkeley (2000).
6. R.M. Clarke et al.: In *Proceedings of the Second International Workshop on the Identification of Dark Matter*, ed. by N.J.C. Spooner, V. Kudryavtsev (World Scientific, Singapore 1999).
7. R.M. Clarke: Ph. D. thesis, Stanford University, Stanford (1999).
8. R.M. Clarke et al.: Appl. Phys. Lett. **76**, 2958 (2000).
9. T. Shutt et al.: Nucl. Instrum. Meth. **A 444**, 340 (2000).
10. A. Da Silva *et al.*, *Nucl. Instrum. Meth.* **A 354**, 553 (1995).
11. R. Abusaidi *et al.*, *Phys. Rev. Lett.* **84**, 5699 (2000).
12. R. Bernabei *et al.*, *Phys. Lett.* B **480**, 23 (2000).
13. G.J. Feldman and R.D. Cousins, *Phys. Rev.* D **57**, 3873 (1998).
14. J.D. Lewin, P.F. Smith: Astropart. Phys **6**, 87 (1996).
15. R. Gaitskell and V. Mandic, *http://dmtools.berkeley.edu/*.